Ionics (2021) 27:1853–1860
https://doi.org/10.1007/s11581-021-04015-y

ORIGINAL PAPER

Cycling properties of $Na_3V_2(PO_4)_2F_3$ as positive material for sodium-ion batteries

Nicolò Pianta[1] · Davide Locatelli[1] · Riccardo Ruffo[1,2]

Received: 29 January 2021 / Revised: 28 February 2021 / Accepted: 20 March 2021 / Published online: 2 April 2021

Abstract

The research into sodium-ion battery requires the development of high voltage cathodic materials to compensate for the potential of the negative electrode materials which is usually higher than the lithium counterparts. In this framework, the polyanionic compound $Na_3V_2(PO_4)_2F_3$ was prepared by an easy-to-scale-up carbothermal method and characterized to evaluate its electrochemical performances in half cell vs. metallic sodium. The material shows a specific capacity (115 mAh g^{-1}) close to the theoretical limit, good coulombic efficiency (>99%) and an excellent stability over several hundred cycles at high rate. High-loading free-standing electrodes were also tested, which showed interesting performances in terms of areal capacity and cyclability.

Keywords Fluorophosphates · NASICON · Sodium-ion battery · Positive electrodes · Self-standing electrodes

Introduction

Nowadays, rechargeable batteries are fundamental for both static and mobile applications. With their long-term history and deep investigations, lithium-ion batteries (LIBs) rule the landscape of electrochemical energy storage, but this may change in the future due to the low abundance of lithium in the earth's crust and its enormous request in order to satisfy the growing battery market [1, 2]. Sodium-ion batteries (NIBs) have been proposed as potential candidates in the replacement of LIBs for several applications thanks to the physico-chemical similarities between the two elements and the abundance and ubiquity of sodium on earth.

There are, however, some differences between the two ions, reflected in their electrochemical properties such as the higher molar mass (23.2 and 6.9 g mol^{-1} for sodium and lithium, respectively) and the higher standard reduction potential (−2.71 and −3.04 V vs. SHE) which leads to lower energy densities [3]. While it is true that the weight of cyclable Na^+ and Li^+ are just a small fraction of the mass of the whole electrodes (no practical penalty in terms of energy density loss) [4], it is clear that the electrode potential gap (about 300 mV) needs to be considered to make NIBs competitive to LIBs. Moreover, sodium's bigger radius becomes an issue for the stability of several intercalation cathodic materials, such as layered oxides. For example, while the intercalation process takes place in $Li_{1-x}CoO_2$ with a narrow potential range (from 4.3 to 3.5 vs. Li^+/Li for x=0.5), Na_xCoO_2 is characterized by several drops of the insertion potential of Na^+ during reduction [5]. This is to attribute to the several changes in the oxide's structure to better accommodate sodium ions, resulting in an overall cathodic potential that is generally about 1V less with respect of lithium's counterpart, thus affecting the energy density of the full battery. In order to overcome these issues, it is necessary to focus on different solutions, such as high voltage cathodic materials which can be achieved, for example, with polyanionic compounds.

Since the use of olivine ($LiFePO_4$) for LIBs, the phosphate anion has been widely studied for both lithium and sodium-ion batteries due to its intrinsic thermal stability. Furthermore, when partially substituted with fluoride, the resulting network allows for a higher insertion electrical potential of alkali ions, due to the stabilization of the

This paper is dedicated to the late Professor Claudio Maria Mari, who inspired the research here reported

✉ Riccardo Ruffo
riccardo.ruffo@unimib.it

[1] Dipartimento di Scienza dei Materiali, Università di Milano Bicocca, 20125 Milano, Italy

[2] National Reference Center for Electrochemical Energy Storage (GISEL) - Consorzio Interuniversitario Nazionale per la Scienza e Tecnologia dei Materiali (INSTM), 50121 Firenze, Italy

antibonding d-orbitals of the metal thanks to the inductive effect in the M-F bond [6]. For those reasons, nowadays fluorophosphate materials are considered valid alternatives to transition metal oxides.

Several phosphates and fluorophosphates have been proposed during the past years, such as $Na_3V_2(PO_4)_3$ (operating voltage of ~3.4V Na^+/Na) [7], Na_2FePO_4F (operating voltage ~3.5V vs. Li^+/Li) [8], $NaVPO_4F$ (operating voltage of ~3.7V vs. hard carbon in a SIB) [9] and $Na_3M_2(PO_4)_2F_3$ (with M = Ti, Fe, V) [10, 11]. Among all these materials, $Na_3V_2(PO_4)_2F_3$ shows the highest potential against metallic sodium (~3.8V) and a relatively high theoretical capacity of 128.3 mAh g^{-1}. With its tetragonal crystal lattice ($P4_2/mnm$), it has channels in which Na^+ ions can move fast, and it is to be considered a NASICON-like structure. However, the separation of vanadium ions by the phosphates combined with the strong ionicity of the V-F bond leave this material with poor electronic conductivity.

The $Na_3V_2(PO_4)_2F_3$ phase (NVPF) was firstly prepared by J. Barker in 2006 [11] using the carbothermal reduction. In further works of the same group [12, 13], the material was tested in half lithium cells, i.e. after the first in situ desodiation, it was evaluated as positive material for LIBs. The preliminary results in Na^+ ion electrolyte were not so promising [13]. The first example of successful use in Na half cell was reported in 2012 using 1 M $NaClO_4$ as electrolyte [14]. Despite the ball milling process with 20% of carbon and the low electrode loading (1.85 mg cm^{-2}), the material was able to provide 110 mAh g^{-1} at low current. A rate test was performed; however, no data were reported about cyclability. Subsequently, several electrolytes were tested, both in half cell vs. Na and full cells with hard carbon [15]. However, the electrode was fabricated with a large amount of carbon (27%) and low mass loading (2 mg cm^{-2}). An improved preparation route, also based on carbothermal reduction, was presented in 2014 [16]. The electrodes were fabricated with 80% of active material with higher mass loading (4.5 mg cm^{-2}), and the diffusion coefficient was investigated. Cyclability tests were performed with materials obtained by sol gel [17] and wet chemistry [18]. Electrodes were produced with 70% of active material and a mass loading of 1.5/2.0 mg cm^{-2}, and they showed remarkable cyclability and rate capabilities (more than 1000 cycles at C/rate of 10C or higher) obtained thanks to the use of carbon shells [17] or nanocomposites [18]. The only example of high load electrode (about 10 mg cm^{-2}) was reported in 2017, showing promising results but without presenting cyclability data [19]. More recent works focused on the composite preparation (e.g. with graphene oxide [20]) without further investigating the pristine materials.

From the literature analysis, it is clear that the carbothermal synthesis seems to be the more suitable and scalable method for preparing materials and simultaneously disperse them inside a carbonaceous (conductive) matrix. The aim of this work was to reproduce and optimize the synthetic procedure to produce NVPF active materials, which are then formulated in electrodes with different mass loads and tested to report the corresponding rate capabilities. A long cycling test is also reported. Moreover, as attempt to produce high load electrodes (> 20 mg cm^{-2}), we report the result about a NVPF free-standing membrane which can be processed from aqueous solution.

Materials and methods

$Na_3V_2(PO_4)_2F_3$ was prepared with a slightly modified procedure as what suggested by Weixin et al. [16]. Firstly, stochiometric amounts of $NH_4H_2PO_4$, V_2O_5 and NaF were dissolved/dispersed in distilled water, stirred and dried under air flux at 50°C. Then, 5 wt% of Super P as a carbon source was grounded with the other reagents with a mortar. The resulting powders were pelletized and heated in argon atmosphere in a single synthesis composed by two steps: the first at 350°C for 4h and the second at 650°C for 8h. The two-step heating procedure was introduced to form oxides and phosphate (first step) and then promote the reaction between them (second step). Between the two treatments, we ground and pelletize the precursors in order to make the contact between them more homogenous and intimate.

As-synthesized powders were studied with X-ray powder diffraction (XRD), performed with a Rigaku Miniflex 600. The analysis was made from 10 to 80 degrees (2θ) with a step size of 0.02 degrees, an angular velocity of 0.1 degrees per minute and using a copper source. Scanning electron microscopy was performed with a Zeiss® Gemini SEM 450. Even though all samples (powder and electrodes) had some content of carbon inside, each of them was covered with graphite in order to reduce the charging effects. Optical images were collected with a Leica® optical microscope equipped with a Leica DFC280 digital colour camera.

Electrodes' slurries were prepared by mixing together the active material (80 wt%) with Super P 10 wt%) and PVdF (10 wt%) as binder, using NMP as solvent. The resulting slurries were deposited on aluminium foils (30 μm of thickness) with different thicknesses (5, 10 and 30 mils), then dried under vacuum at 80°C overnight and pressed with a calender. Self-standing high-load electrodes were prepared following a previously reported route [21] by grounding NVPF together with Super P conductive carbon in a mortar and mixing the obtained

powder with a suspension of PTFE in water (Sigma-Aldrich, 60 wt%) to obtain a homogenous dough. The amount of suspension was calculated in order to have the same ratio of active material/binder as for the supported electrode, i.e. 8:1. The dough was then calendered several times reducing the thickness up to obtain a flexible film with final thickness of 180 μm. R2032 coin cells were assembled in an argon-filled glove box, using metallic sodium as counter electrode and a 1M solution of $NaClO_4$ in PC + FEC (2 wt%) as electrolyte, and were tested using a Bio-Logic VMP3 battery tester.

Results and discussion

X-ray diffraction technique has been used both for evaluating the preparation products and the presence of impurities. As shown in Fig. 1, the Rietveld refinement shows that the main phase is NVPF (97%), with a small amount of $Na_3V_2(PO_4)_3$ (NVP) as impurity. The average particle dimension of crystallites was also evaluated by means of the Scherrer equation, obtaining a value of about 45 nm, considering the two most intense (002) and (222) peaks.

SEM images of the as-synthesized NVPF powders are shown in Fig. 2 together with the histogram of the particle size obtained by averaging different images. The microstructure consists nano-sized particles with dimension picked around 60–80 nm but partially coalesced in agglomerations of few micrometres. The residual carbon left from carbothermal reduction reaction was evaluated with CHNS measurement, corresponding to 5.4% of the whole mass.

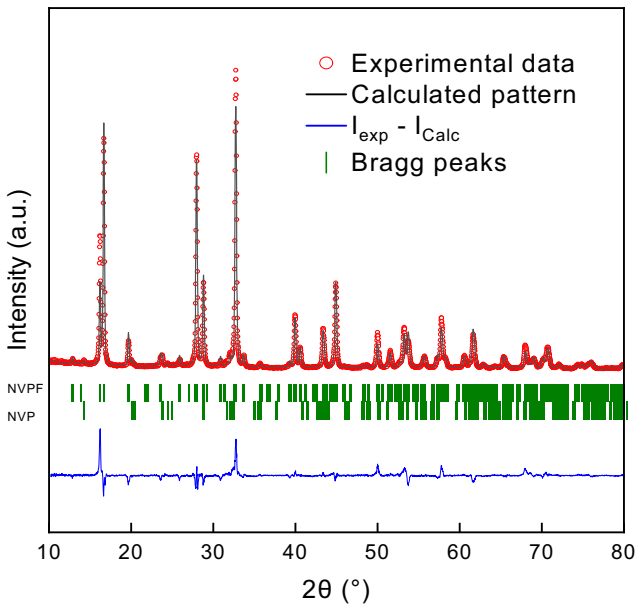

Fig. 1 XRD pattern of the obtained powders NVPF (red dots) and Rietveld results using the $Na_3V_2(PO_4)_2F_3$ and $Na_3V_2(PO_4)_3$ reference materials

The morphological features of supported and free-standing electrodes were characterized by optical and electronic microscopy (Fig. 3). The Al-supported electrode (Fig. 3a) shows a compact surface with an overall good homogeneity. The electrode's thickness was evaluated via optical microscopy (insertion in Fig. 3a), showing a total average thickness of about 49±4 μm (34±4 μm excluding the aluminium foil). At higher magnification (Fig. 3b), it is possible to appreciate the binder filaments, while it is harder to distinguish between active materials and Super P particles. The self-standing electrode (Fig. 4a) seems porous and homogenous in composition; also in this case (Fig. 4b), the binder filaments are clearly observed. The electrode thickness is constant and it has been measured as 237±7 μm.

The quasi-thermodynamic electrochemical behaviour of $Na_3V_2(PO_4)_2F_3$ was explored with PCGA (potentiodynamic cycling with galvanostatic acceleration) technique. The measurement was indeed performed by applying potentiostatic steps of 4 mV until the current dropped below a limit value (in our case 0.02C, 2.56 mA g^{-1}). This procedure allows to extract/insert sodium inside the structure with very little overpotentials, thus operating near the equilibrium, and collecting all the available charge thanks to the low current threshold. Figure 4a depicts the voltage-capacity curves of three cycles of sodiation/desodiation of NVPF. As expected, the reaction with sodium happens at three different potentials, roughly 3.4V, 3.6V and 4.0V vs. Na^+/Na. These electrochemical events are better shown in the differential capacity curves derived from PCGA (Fig. 4b). As stated by Weixin et al. [16], the two low-potential peaks are associated to the insertion/extraction of the first equivalent of sodium through a two-phase reaction, while the highest peaks involve the second equivalent of Na^+ in a mono-phase domain. This can easily be appreciated from the shape of the peaks which appear sharp-spiked and broad-bellied for the low and potential processes, respectively. From PCGA it was also possible to calculate the mean potential at which NVPF operates with very low overpotentials. This value was calculated in the half cell using the ratio between the energy (the integral of the V/charge curve) and the capacity, both obtained during sodiation/desodiation, respectively. For the cathodic sodiation, NVPF operates at a mean operative potential of 3.78 V. The total charge stored in the material is 120 mAh g^{-1}, a value close to the theoretical one. However, during the first desodiation, an irreversible capacity of about 30 mAh g^{-1} is observed due probably to the formation of the cathodic electrolyte interface (CEI) on both the active materials and the carbon additive [22, 23].

The kinetic behaviour of NVPF was observed by means of galvanostatic measurements. Figure 4c shows

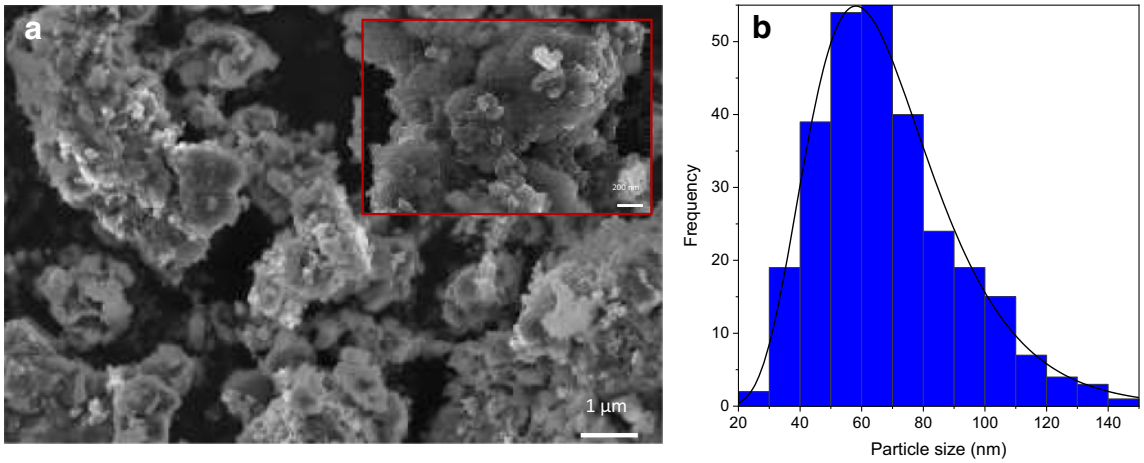

Fig. 2 (**a**) SEM images of as-synthesized NVPF taken at different magnitudes (10k and 50k, respectively) and (**b**) particle size distribution histogram

the achieved capacity obtained during subsequent cycling at different currents (0.1C, 0.2C, 0.5C, 1C, 5C and 10C). Achievable capacity showed an inverse proportion with respect to the C-rate, losing about 20% (88 mAh g^{-1} with respect to the starting value of 110 mAh g^{-1}) after increasing the current from 0.1C to 1C, but with an increase in the coulombic efficiency (> 99%), as an indication of the presence of anodic parasitic reactions. Moreover, NVPF showed a very good capacity recovery after high currents cycling as well as stability. When returning to 0.1C, indeed, the capacity resets back to 105 mAh g^{-1}, which is 95% of the initial value, and then decreased less than 3 mAh g^{-1} during the next 50 cycles at low currents. Mean potentials were also evaluated for each cycle (Fig. 4d). NVPF showed relatively low polarization at low C-rates, with an increase of the mean potential of about 60–70 mV between scanning at 0.1C and 1C, while higher overpotentials (200/400 mV) can be seen for currents of

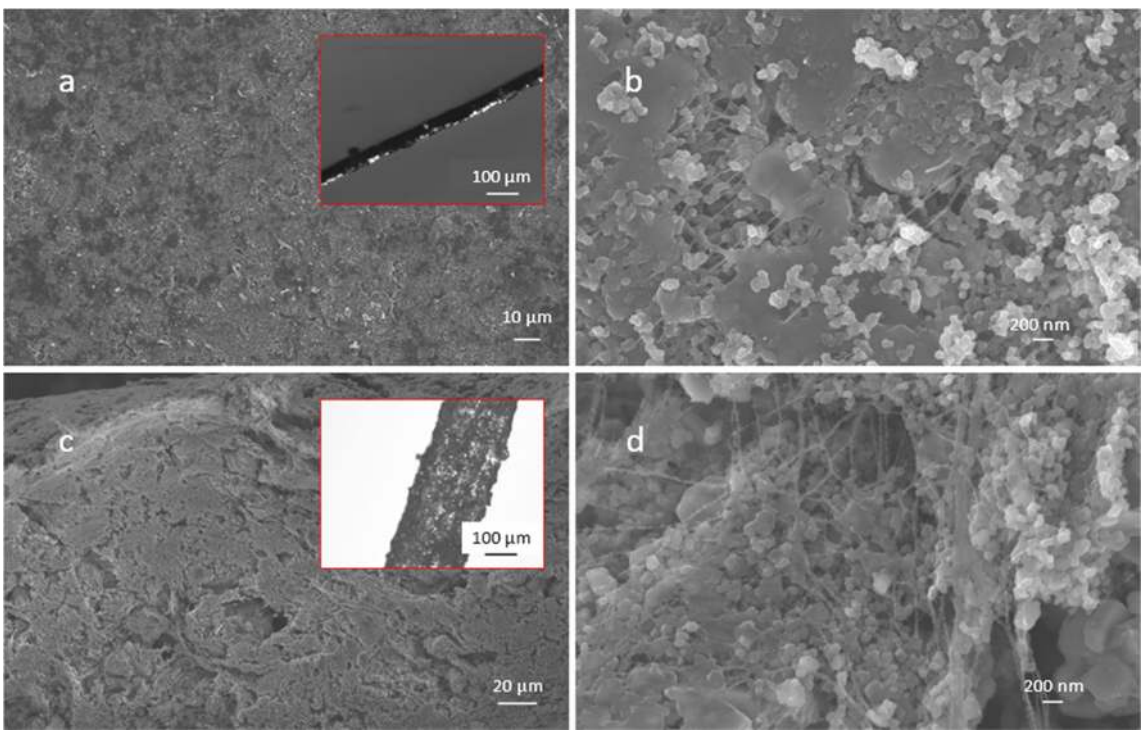

Fig. 3 Images of the two electrodes' configuration Al-supported and self-standing. (**a**, **b**) SEM images of the Al-supported electrode. (**c**, **d**) SEM images of the self-standing one. The two inserted images are optical microscope's images of the cross section of the two electrodes

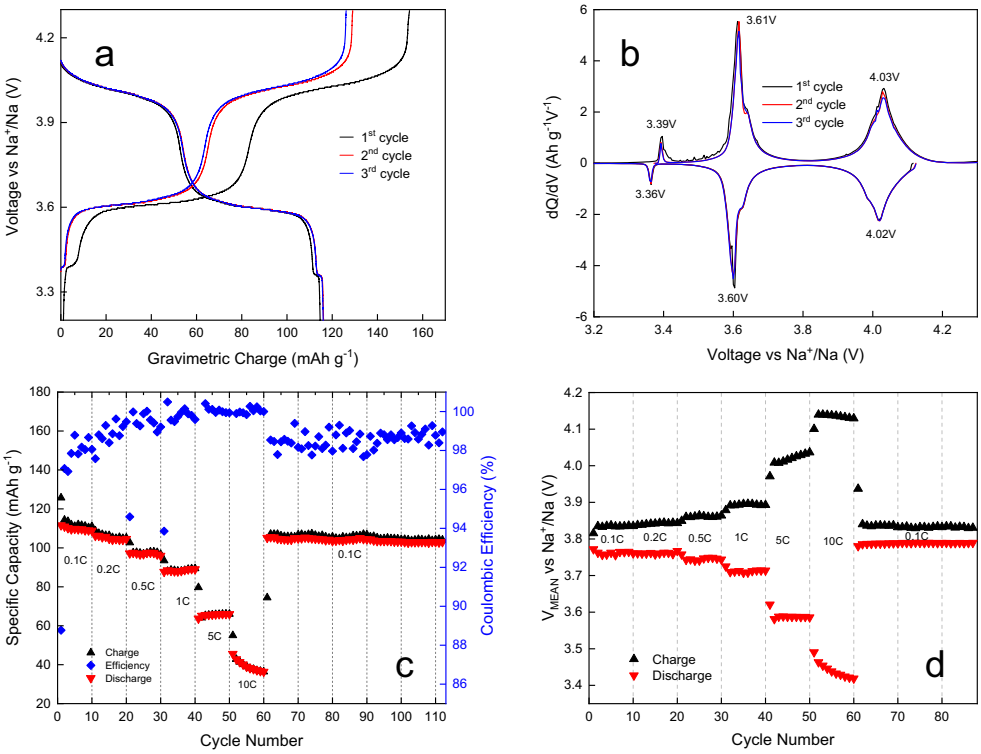

Fig. 4 (**a**) Voltage-gravimetric charge curves of PCGA measurement. (**b**) Differential capacities curves derived from PCGA. (**c**) Specific capacity vs. cycle number for NVPF at various C-rates. (**d**) Sodiation and desodiation mean voltages vs. cycle number

5C and 10C. The stable trend of the mean potential (3.78V) during recovery cycles means that NVPF does not undergo irreversible changes in structure during multiple sodiations/desodiations. This can be considered another good indication of NVPF's stability and cyclability.

To better evaluate the stability of NVPF during cycles, a long-term measurement was performed: starting from 0.1C then increasing current to 1C and, in the end, 2C. As displayed in Fig. 5, this material showed outstanding stability performances, with very high cyclability (more than

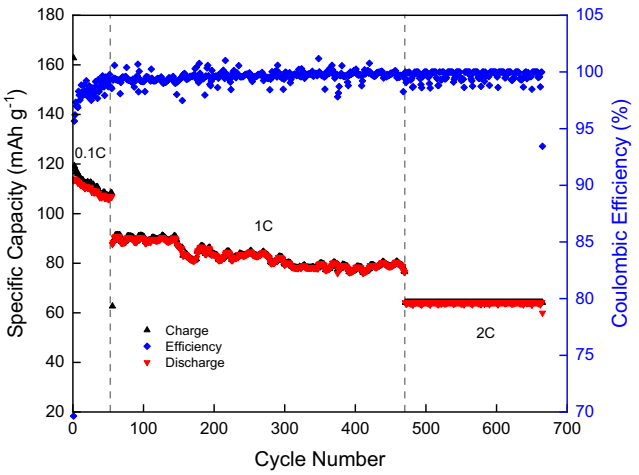

Fig. 5 Specific capacity vs. cycle number for a long-term cycling of NVPF

600 cycles in total and almost zero loss of specific capacity at 2C) and high coulombic efficiencies of more than 99% at 1C and 2C.

Electrodes with different mass loading of active materials were also tested. Figure 6a displays the discharge capacity of three electrodes with different mass loadings, 1.5, 3.5 and 6.4 mg cm^{-2}, respectively, using a common cycling procedure (10 cycles at C-rates of 0.1, 0.2, 0.5, 1, 5, 10 and again 0.1). At low currents, where kinetical effects tend to be negligible and thus materials operate in conditions that are not too far from the thermodynamic limit, the three electrodes showed no significant differences. This may suggest that NVPF could be very well dispersed inside the carbonaceous matrix (from electrode formulation but also from carbothermal reduction), increasing electronic conductivity and thus reducing overpotentials. Still, deviations of capacity retention are present at high currents, where kinetic effects tend to reduce specific capacity values in electrodes with higher thickness and larger mass loading. Same trends can be observed for both coulombic efficiencies and mean operative voltages.

Finally, the self-standing, very high mass-loading electrodes (25 mg cm^{-2}) were also tested and compared to the aluminium-supported ones. Despite working at a much higher current (almost four times), self-standing electrodes showed identical performances in terms of specific capacity and cyclability at low C-rates (0.1 and 0.2C, Fig. 7)

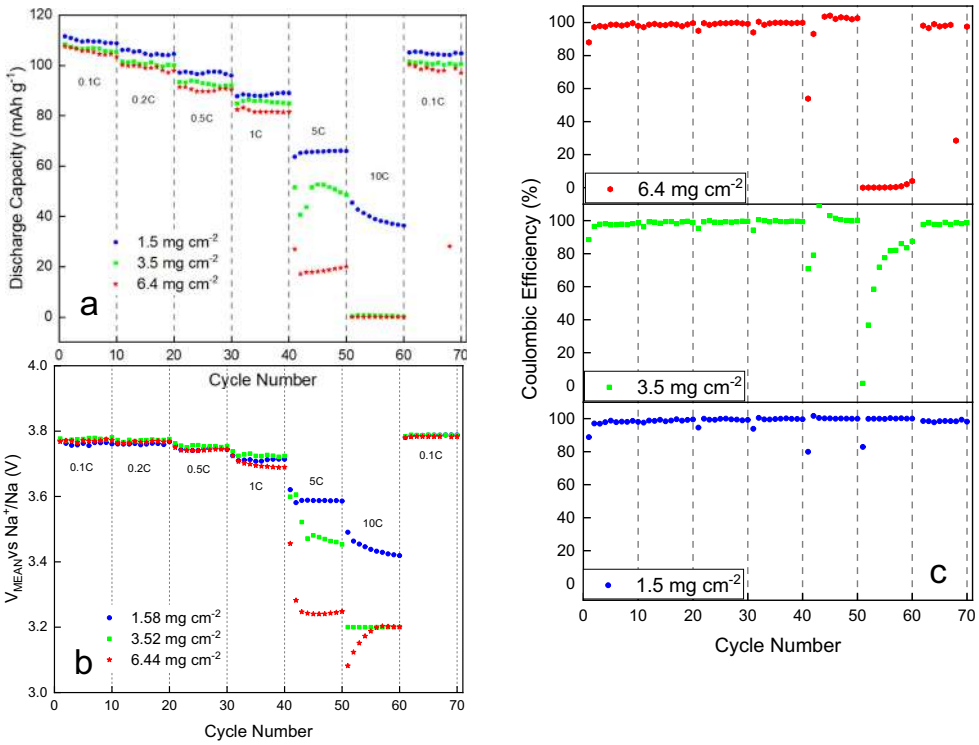

Fig. 6 Comparison among electrodes with different loadings of active mass during cycling. (**a**) Cathodic specific capacity. (**b**) Mean discharge voltage. (**c**) Coulombic efficiency

while failing at higher currents. This can be due to inefficiencies in the working electrode itself but also to issues in the sodium counters used in the half cells that tend to form thick SEI layers as well as dendrites at high currents during to the long operation of the cell. Still, self-standing electrodes can be considered good candidates for full cell NIBs because of the capacity (neither affected by the high mass nor by the absence of the current collector), the coulombic efficiency (> 98–99% even at low C-rates) and the average voltage (3.8V vs. Na^+/Na). The obtained areal capacities of the self-standing and the 6.4 g cm^{-2} electrodes are 2.45 and 0.65 mAh cm^{-2}, respectively.

Conclusions

$Na_3V_2(PO_4)_2F_3$ was prepared by means of a carbothermal reduction synthesis with high crystallinity. A small amount of NVP impurity was detected (3%). The material showed good performances as a positive electrode for sodium-ion batteries able to operate at a mean voltage of almost 3.8 V under quasi-thermodynamic conditions. Low load electrodes also showed outstanding cyclability properties with coulombic efficiency always above 98–99%. The stable trend of the mean voltage, with relatively low overvoltage at current up to 1C, makes this material

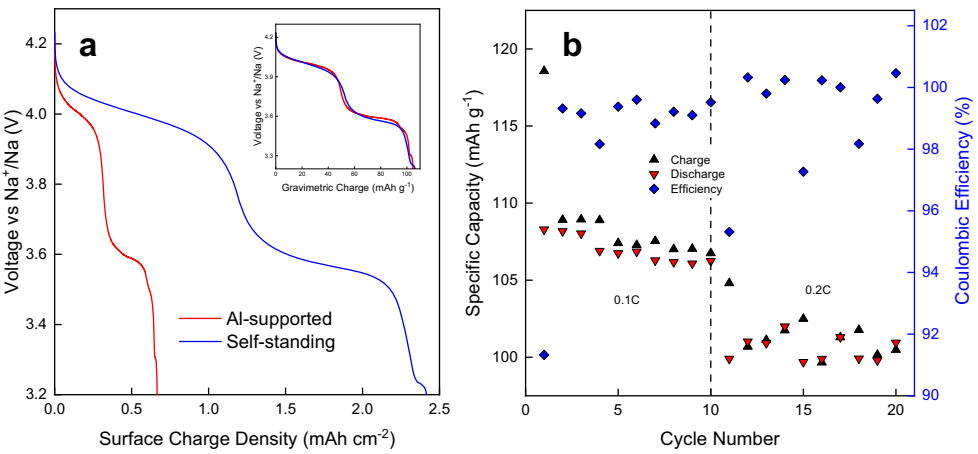

Fig. 7 Comparison between Al-supported (active mass loading: 6.4 mg cm^{-2}) and self-standing (active mass loading: 25 mg cm^{-2}) electrodes. (**a**) Surface charge density of the 5th cycle for both systems with the gravimetric charge as insert and (**b**) specific capacity for the self-standing electrode at two different C-rates (0.1 and 0.2C)

suitable for low-to-mid power delivery systems, and it is also a factor that affects the energy efficiency, which maintains higher than 94%. Moreover, NVPF synthesized by carbothermal reduction appeared to be conductive enough in order to allow low-to-no kinetical effects when increasing mass loadings on electrodes. This is particularly true considering that even self-standing electrodes with high thicknesses (180 μm) and high mass loadings (25 mg cm^{-2}) show very good performances in terms of coulombic efficiency and achieved capacity.

Funding Open access funding provided by Università degli Studi di Milano - Bicocca within the CRUI-CARE Agreement. This work has been funded by the Italian Ministry of University and Research (MIUR) through grants "Dipartimenti di Eccellenza 2017 – Materials for energy" and PRIN 2017 "Towards sustainable, high-performing, all-solid-state sodium-ion batteries".

Declarations

Conflict of interest The authors declare no competing interests.

References

1. Armand M, Tarascon JM (2008) Building better batteries. Nature 451:652–657. https://doi.org/10.1038/451652a
2. Zu CX, Li H (2011) Thermodynamic analysis on energy densities of batteries. Energy Environ Sci 4:2614–2624. https://doi.org/10.1039/c0ee00777c
3. Hwang JY, Myung ST, Sun YK (2017) Sodium-ion batteries: present and future. Chem Soc Rev 46:3529–3614. https://doi.org/10.1039/c6cs00776g
4. Slater MD, Kim D, Lee E, Johnson CS (2013) Sodium-ion batteries. Adv Funct Mater 23:947–958. https://doi.org/10.1002/adfm.201200691
5. Berthelot R, Carlier D, Delmas C (2011) Electrochemical investigation of the P2-NaxCoO2 phase diagram. Nat Mater 10:74–80. https://doi.org/10.1038/nmat2920
6. Arroyo y de Dompablo ME, Amador U, Tarascon JM (2007) A computational investigation on fluorinated-polyanionic compounds as positive electrode for lithium batteries. J Power Sources 174:1251–1257. https://doi.org/10.1016/j.jpowsour.2007.06.178
7. Jian Z, Zhao L, Pan H, Hu YS, Li H, Chen W, Chen L (2012) Carbon coated Na3V2(PO4)3 as novel electrode material for sodium ion batteries. Electrochem Commun 14:86–89. https://doi.org/10.1016/j.elecom.2011.11.009
8. Ellis BL, Makahnouk WRM, Makimura Y, Toghill K, Nazar LF (2007) A multifunctional 3.5V iron-based phosphate cathode for rechargeable batteries. Nat Mater 6:749–753. https://doi.org/10.1038/nmat2007
9. Navpo F, Barker J, Saidi MY, Swoyer JL (2003) A sodium-ion cell based on the fluorophosphate compound NaVPO4F. Electrochem Solid-State Lett 6:11–14. https://doi.org/10.1149/1.1523691
10. Chihara K, Kitajou A, Gocheva ID, Okada S, Yamaki JI (2013) Cathode properties of Na3M2(PO4)2F3[M = Ti, Fe, V] for sodium-ion batteries. J Power Sources 227:80–85. https://doi.org/10.1016/j.jpowsour.2012.10.034
11. Barker J, Saidi MY, Swoyer JL, (2002) US Patent 6, 387,568
12. Gover RKB, Bryan A, Burns P, Barker J (2006) The electrochemical insertion properties of sodium vanadium fluorophosphate, Na3V2(PO4)2F3. Solid State Ionics 177:1495–1500. https://doi.org/10.1016/j.ssi.2006.07.028
13. Barker J, Gover RKB, Burns P, Bryan AJ (2007) Li4 3Ti5 3O4‖Na3V2(PO4)2F3: an example of a hybrid-ion cell using a non-graphitic anode. J Electrochem Soc 154:A882–A887. https://doi.org/10.1149/1.2756975
14. Shakoor RA, Seo DH, Kim H, Park YU, Kim J, Kim SW, Gwon H, Lee S, Kang K (2012) A combined first principles and experimental study on Na3V2(PO4)2F3 for rechargeable Na batteries. J Mater Chem 22:20535–20541. https://doi.org/10.1039/c2jm33862a
15. Ponrouch A, Dedryvère R, Monti D, Demet AE, Ateba Mba JM, Croguennec L, Masquelier C, Johansson P, Palacín MR (2013) Towards high energy density sodium ion batteries through electrolyte optimization. Energy Environ Sci 6:2361–2369. https://doi.org/10.1039/c3ee41379a
16. Song W, Ji X, Wu Z, Yang Y, Zhou Z, Li F, Chen Q, Banks CE (2014) Exploration of ion migration mechanism and diffusion capability for Na3V2(PO4)2F3 cathode utilized in rechargeable sodium-ion batteries. J Power Sources 256:258–263. https://doi.org/10.1016/j.jpowsour.2014.01.025
17. Liu Q, Wang D, Yang X, Chen N, Wang C, Bie X, Wei Y, Chen G, du F (2015) Carbon-coated Na3V2(PO4)2F3 nanoparticles embedded in a mesoporous carbon matrix as a potential cathode material for sodium-ion batteries with superior rate capability and long-term cycle life. J Mater Chem A 3:21478–21485. https://doi.org/10.1039/c5ta05939a
18. Liu Q, Meng X, Wei Z, Wang D, Gao Y, Wei Y, du F, Chen G (2016) Core/double-shell structured Na3V2(PO4)2F3@C nanocomposite as the high power and long lifespan cathode for sodium-ion batteries. ACS Appl Mater Interfaces 8:31709–31715. https://doi.org/10.1021/acsami.6b11372
19. Bianchini M, Xiao P, Wang Y, Ceder G (2017) Additional sodium insertion into polyanionic cathodes for higher-energy na-ion batteries. Adv Energy Mater 7:1–9. https://doi.org/10.1002/aenm.201700514
20. Cai Y, Cao X, Luo Z, Fang G, Liu F, Zhou J, Pan A, Liang S (2018) Caging Na3V2(PO4)2F3 microcubes in cross-linked graphene enabling ultrafast sodium storage and long-term cycling. Adv Sci 5:1800680. https://doi.org/10.1002/advs.201800680
21. Tribbia M, Pianta N, Brugnetti G, Lorenzi R, Ruffo R (2020) A new double layer super-capacitor made by free-standing activated carbon membranes and highly concentrated potassium acetate solutions. Electrochim Acta 364:137323. https://doi.org/10.1016/j.electacta.2020.137323

22. Chen Y, Zhang D, Bian X, Bie X, Wang C, du F, Jang M, Chen G, Wei Y (2012) Characterizations of the electrode/electrolyte interfacial properties of carbon coated Li 3 V 2 (PO 4) 3 cathode material in LiPF 6 based electrolyte. Electrochim Acta 79:95–101. https://doi.org/10.1016/j.electacta.2012.06.082
23. Li W, Dolocan A, Oh P, Celio H, Park S, Cho J, Manthiram A (2017) Dynamic behaviour of interphases and its implication on high-energy-density cathode materials in lithium-ion batteries. Nat Commun 8:1–10. https://doi.org/10.1038/ncomms14589